

AD-A104 680

AEROSPACE CORP EL SEGUNDO CA LAB OPERATIONS
THERMAL EXPANSION OF METAL MATRIX COMPOSITES.(U)
AUG 81 E G WOLFF

F/6 11/4

UNCLASSIFIED

TR-0081(6950-01)-1

SD-TR-81-56

F04701-80-C-0081

NL

1 OF 1
40 A
0480

END
DATE
FILMED
10-81
DTIC

LEVEL

(12) PS

AD A104680

Thermal Expansion of Metal Matrix Composites

Prepared by
E. G. WOLFF
Laboratory Operations
The Aerospace Corporation
El Segundo, Calif. 90245

DTIC
ELECTE
SEP 29 1981
S D H

1 August 1981

APPROVED FOR PUBLIC RELEASE;
DISTRIBUTION UNLIMITED

FILE COPY


Prepared for
SPACE DIVISION
AIR FORCE SYSTEMS COMMAND
Los Angeles Air Force Station
P.O. Box 92960, Worldway Postal Center
Los Angeles, Calif. 90009


81 9 28 150

This report was submitted by The Aerospace Corporation, El Segundo, CA 90245, under Contract No. F04701-80-C-0081 with the Space Division, Deputy for Technology, P.O. Box 92960, Worldway Postal Center, Los Angeles, CA 90009. It was reviewed and approved for The Aerospace Corporation by W. C. Riley, Director, Materials Sciences Laboratory. Major Ralph R. Gajewski, SD/YLXT, was the project officer for the Mission Oriented Investigation and Experimentation (MOIE) Program.

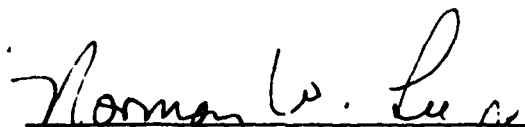
This report has been reviewed by the Public Affairs Office (PAS) and is releasable to the National Technical Information Service (NTIS). At NTIS, it will be available to the general public, including foreign nations.

This technical report has been reviewed and is approved for publication. Publication of this report does not constitute Air Force approval of the report's findings or conclusions. It is published only for the exchange and stimulation of ideas.


Ralph R. Gajewski, Major, USAF
Project Officer


Florian P. Meinhardt, Lt Col, USAF
Director, Directorate of Advanced
Space Development

FOR THE COMMANDER


Norman W. Lee Jr., Colonel, USAF
Deputy for Technology

UNCLASSIFIED

SECURITY CLASSIFICATION OF THIS PAGE (When Data Entered)

REPORT DOCUMENTATION PAGE		READ INSTRUCTIONS BEFORE COMPLETING FORM	
1. REPORT NUMBER SD-TR-81-56	2. GOVT ACCESSION NO. AD-A204680	3. RECIPIENT'S CATALOG NUMBER	
4. TITLE (and Subtitle) THERMAL EXPANSION OF METAL MATRIX COMPOSITES		5. TYPE OF REPORT & PERIOD COVERED Tech. rept.	
7. AUTHOR(s) E. G. Wolff		6. PERFORMING ORG. REPORT NUMBER TR-0081(6950-01)-1	
9. PERFORMING ORGANIZATION NAME AND ADDRESS The Aerospace Corporation El Segundo, California 90245		8. CONTRACT OR GRANT NUMBER(s) F04701-80-C-0081	
11. CONTROLLING OFFICE NAME AND ADDRESS Space Division Air Force Systems Command Los Angeles, California 90009		10. PROGRAM ELEMENT, PROJECT, TASK AREA & WORK UNIT NUMBERS	
14. MONITORING AGENCY NAME & ADDRESS (if different from Controlling Office) 1721		12. REPORT DATE 1 August 1981	
		13. NUMBER OF PAGES 42	
		15. SECURITY CLASS. (of this report) Unclassified	
		15a. DECLASSIFICATION/DOWNGRADING SCHEDULE	
16. DISTRIBUTION STATEMENT (of this Report) Approved for public release; distribution unlimited.			
17. DISTRIBUTION STATEMENT (of the abstract entered in Block 20, if different from Report)			
18. SUPPLEMENTARY NOTES			
19. KEY WORDS (Continue on reverse side if necessary and identify by block number) composites graphite-magnesium metal matrix laser interferometry thermal expansion thermal cycling graphite-aluminum			
20. ABSTRACT (Continue on reverse side if necessary and identify by block number) Metal matrix composites offer numerous options in materials performance over the more conventional resin matrix composites; consequently, it is necessary to obtain a complete data base on this class of materials. In this report are described methods and results of thermal expansion measurements. Because theoretical predictions indicate that very low expansion values can be achieved, there is an interest in related thermal measurements, such as thermal cycling behavior, the effects of internal stresses, and microcracking. In particular,			

DD FORM 1473
(FACSIMILE)

UNCLASSIFIED

SECURITY CLASSIFICATION OF THIS PAGE (When Data Entered)

UNCLASSIFIED

SECURITY CLASSIFICATION OF THIS PAGE(When Data Entered)

19. KEY WORDS (Continued)

+ 11-00000001

20. ABSTRACT (Continued)

there must be adequate experimental accuracy to measure these quantities as a function of fiber-metal system.

The advantages of essentially contactless measurement techniques such as Michelson interferometers are presented, including a lack of restriction on sample size or shape. The special requirements in laser characteristics, optics, gaseous and thermal environments, signal processing, and data reduction needed to describe fully low thermal expansion behavior are outlined. Dimensional changes must be measured with an accuracy on the order of $\pm 10^{-8}$ m.

Since differential thermal strains between fiber and matrix have been found to produce stresses that exceed the transverse strength of resin matrixes, a new acousto-optical technique is employed to study microcracking in metal matrix composites at low temperatures, concurrently with coefficient of thermal expansion (CTE) measurements. The instrumentation required to analyze high-frequency signals in laser interferometers is described.

Experimental results are presented for B-Al, graphite-Al, SiC/Al and graphite-Mg composites. It is shown that the macroscopic thermal expansion properties can be reasonably predicted when the value of E_f after fabrication is reliably known, for example, when the composite value E_c conforms to the rule of mixtures. The fine structure of a length-versus-temperature curve requires more detailed analysis, and the possible effects of plastic flow, microcracking, and other thermal fatigue phenomena, such as delaminations, must be considered.

UNCLASSIFIED

SECURITY CLASSIFICATION OF THIS PAGE(When Data Entered)

CONTENTS

I.	INTRODUCTION.....	7
II.	THEORY.....	9
III.	EXPERIMENTAL TECHNIQUES.....	15
IV.	RESULTS.....	27
	A. Graphite-Al.....	27
	B. Graphite-Mg.....	32
	C. Silicon Carbide-Al.....	42
V.	SUMMARY.....	43
	REFERENCES.....	45

Accession For	
NTIS GRA&I	<input checked="" type="checkbox"/>
DTIC TAB	<input type="checkbox"/>
Unannounced	<input type="checkbox"/>
Justification	<input type="checkbox"/>
By _____	
Distribution _____	
Available _____	
Dist _____	
A	

FIGURES

1.	Two-Channel Michelson Laser Interferometer.....	16
2.	Thin Test Sample Inside Two-Channel Michelson Interferometer.....	18
3.	Typical Photodetector Output from Two Channel Michelson Interferometer.....	20
4.	Apparatus for Thermal Expansion Testing of Thin Wires, Plates, or Fibers.....	21
5.	Opto-acoustic Recording and Analysis of Microcracking.....	23
6.	Amplitude Versus Frequency from Sample End Vibrations.....	24
7.	CTE Data at 300 K for Unidirectional Graphite-Al Samples Compared with Predictions Based on Eq. (1) and Table 2.....	28
8.	Transverse and Longitudinal Expansion Data for Graphite-Al Composites.....	29
9.	Thermal Cycling Behavior of Unstrained Unidirectional T50/202 Al Composite in the Fiber Direction.	30
10.	Thermal Cycling Behavior for Unidirectional T50/202 Al Prestrained to Its Secondary Modulus (48 ksi) in the Fiber Direction.....	31
11.	CTE Data at 300 K for Unidirectional Graphite-Mg Samples Compared with Predictions Based on Eq. (1) and Table 2.....	33
12.	CTE Data for Unidirectional VS0054-Mg Composite of One-Ply Layer....	36
13.	CTE Data for Unidirectional 50.4% VS0054-Mg Composite of Three-Ply Layers.....	37
14.	CTE Data for Unidirectional 45% VS0054-Mg Composite of Three-Ply Layers.....	38
15.	CTE Data for Unidirectional 38.1% VS0054-Mg Composite of One Layer.....	39
16.	CTE Data for Sample in Fig. 13 at Lower Temperatures.....	40

TABLES

1. Summary of Results of CTE Measurements on Graphite-Mg..... 34
2. Some Properties of Composites Related to CTE..... 35

I. INTRODUCTION*

Metal matrix composites (MMC) offer numerous options in material performance over conventional resin matrix composites, such as high thermal and electrical conductivity and freedom from moisture effects. In many applications where composites are employed as structural materials, the dimensional stability characteristics are of primary concern. Theoretical predictions based on new ultrahigh modulus reinforcing fibers suggest that near-zero thermal expansion coefficients (CTE) are now achievable with metal matrices. The relative importance of related characteristics such as thermal-cycling behavior, internal stress relief, and thermomechanical history is increased. In addition to broadening the data base for MMC, the advances required in theory, measurement techniques, and materials understanding are explored.

There have been few studies of the thermal-cycling behavior of metal matrix composites, and those that exist have emphasized the boron-fiber-reinforced aluminum system.¹⁻⁸ For example, Ferte, Kreider, White, and others^{2,4,5,7} have investigated the effect of elastic-plastic deformation during thermal expansion behavior in B-Al. The matrix yield strength was shown to have a major effect on the CTE. Creep deformation is also common during thermal cycling of graphite-reinforced Al.⁶ In addition to plastic deformation of the matrix, cracking or failure of the fiber and failure of the fiber-matrix interface are all possible. Indeed, matrix cracking of the type found in graphite-epoxy composites is also found in MMC above room temperature. B-Al systems generally have a stronger metal-to-fiber bond than graphite-Al, so that mixed modes of failure are found more frequently in the former system. Graphite-fiber-reinforced metals are characterized by less uniform fiber distribution and a lower transverse strain capability than B-Al. Interply failure may also be possible, especially with weak matrices such as cast alloys or with cross-ply layups. The ductility of a metal may also be expected to influence the low-temperature microcracking behavior.

*The research reported here covers work in this area up to July 1980.

II. THEORY

Predictions of the thermal expansion coefficients (CTE) of composites are based on the work of Turner, Levin, Hill, Hashin, Schapery, Halpin, Pagano, and others.⁹⁻¹⁵ Most of the early work applies to elastic behavior of spherical particles in an isotropic composite and requires bounds set on the bulk modulus through either a uniform-stress or a uniform-strain assumption. In case of a transversely isotropic-aligned fiber composite with two isotropic phases, a number of relations can be shown to be equivalent,⁹ and bounds on the values of the CTE can be obtained from bounds on the moduli. When the Poisson's ratios of the constituents, ν_f and ν_m , are nearly equal, the upper and lower bounds for Levin's original equation¹² reduce to

$$\frac{\overline{E\alpha}}{\overline{E}} < \alpha_o < \frac{\overline{K\alpha}}{\overline{K}} \quad (1)$$

where α_o represents the 0-deg or longitudinal CTE of a unidirectional composite, E the Young's modulus, and K the bulk modulus. The bars denote average quantities. Similarly, the transverse CTE or α_{90} is bounded as:¹⁰

$$\bar{\alpha} < \alpha_{90} < (1 + \nu_f)\alpha_f V_f + (1 + \nu_m)\alpha_m V_m - \alpha_o(\nu_f V_f + \nu_m V_m) \quad (2)$$

where V denotes the volume fraction of the fiber (f) or matrix (m). We have shown¹⁶ that these relations excellently describe thermal expansion behavior in the B-Al system over small temperature excursions near 300 K. For more precise predictions, however, it is necessary to note that while the Poisson's ratios of both B and graphite fibers are generally assumed to be equal to 0.2, there are no direct measurements. Single crystal data for pyrolytic graphite range from -0.15 to 0.9. Dean and Turner¹⁷ show that ν_{ij} values for graphite fibers can range from 0.01 to 0.53. In any case, values of ν_{Al} and ν_{Mg} are

about 0.25 to 0.3. An approach to this problem is suggested by a return to Levin's original equation

$$\alpha_o = \alpha_m + \frac{\alpha_f - \alpha_m}{v_f - v_m} \left[(1 + v_f) (E_o - v_m E_m) - (1 + v_m) v_f E_f \right] \quad (3)$$

using Hill's¹¹ expression for E_o

$$E_o = E_f v_f + E_m v_m + \frac{4v_f v_m (v_f - v_m)^2}{v_f/k_m + v_m/k_f + 1/\mu} \quad (4)$$

where

k = plane-strain bulk modulus

$$k = K + (1/3)\mu \quad (5)$$

$$K = E/3(1-2\nu) \quad (6)$$

$$\mu = E/2(1 + \nu) \quad (7)$$

The subscript for μ in Eq. (4) will be either the fiber or the matrix, thereby setting upper and lower bounds for E in (4) and hence for α_o in (3). Fiber CTE values (α_f) are not known very accurately. There has been an empirical assumption that the negative α_f value is linearly proportional to the elastic modulus (E_f), but in the case of ultrahigh-modulus pitch fibers this may not be true. (Union Carbide reports a value of $-1.26 \times 10^{-6} \text{ K}^{-1}$ for P75S fibers, a value which may be compared with -1.0 to $-1.1 \times 10^{-6} \text{ K}^{-1}$ for GY70 fiber of similar modulus.) In addition to the problem of adequate v_f and α_f values, there is still the assumption in these equations of an isotropic fiber - valid for glass but certainly not for graphite. The effect of anisotropic fibers on the elastic moduli of unidirectional composites has been considered by Hashin,¹⁴ Whitney,¹⁸ and others. An exploration of the bounds on the effective thermal expansion coefficients for isotropic multiphase

composites with anisotropic phases has been made by Rosen and Hashin.^{13,14} In this case, precise knowledge of the various elastic moduli of both phases, as well as Poisson's ratio, is required. Dean,¹⁷ Kriz,¹⁹ and coworkers show that it may be possible to obtain a complete set of mechanical properties with the help of ultrasonic velocity measurements.¹⁹

With both macro- and microscopic isotropy and anisotropic fibers, Hashin¹⁴ gives

$$\alpha_o = \bar{\alpha}_o + (\alpha_{kl}^f - \alpha_{kl}^m) P_{klrs} (S_{rs11}^* - \bar{S}_{rs11}) \quad (8)$$

$$\alpha_{90} = \bar{\alpha}_{90} + (\alpha_{kl}^f - \alpha_{kl}^m) P_{klrs} (S_{rs22}^* - \bar{S}_{rs22}) \quad (9)$$

where S_{rsij} = phase elastic compliances and $P_{klrs} (S_{rsij}^f - S_{rsij}^m) = I_{kl ij}$, a fourth rank symmetric unit tensor. P_{klrs} must be determined by inversion of the transversely isotropic matrix $S_{rsij}^f - S_{rsij}^m$. Hashin shows that in the case of graphite-Al, the assumption of an isotropic fiber leads to the erroneous conclusion that the fiber provides transverse stiffening. In graphite epoxy, in fact, the anisotropic fiber still leads to increases in k , G_o , G_{90} , and E_{90} , but not in the graphite-Al case (G is the shear modulus). The theories discussed are based on linear elastic behavior of all phases of the composites. Kreider and Patarini⁷ point out that changes of $\Delta T > 60K$ are likely to lead to plastic deformation in an Al matrix, which, in turn, accounts for CTE data lower than those predicted by elastic theory. Models to account for matrix yielding effects on CTE have been proposed by Ferte,³ Kreider,⁷ and Neubert.²⁰ In all cases, plastic flow is assumed, with changes in the internal stress states.

For oriented short fiber composites, Halpin¹⁵ gives an approximate equation for the thermal strain e , assuming $\nu_f = \nu_m$:

$$e_o = \alpha_o \Delta T = \bar{e} + \frac{Ee}{E} - \bar{e} \frac{(1/E_L - 1/E_{11})}{(1/E_L - 1/E_u)} \quad (10)$$

where

$$\frac{1}{E_L} = \frac{v_f}{E_f} + \frac{v_m}{E_m} \quad (11)$$

$$E_u = v_f E_f + v_m E_m \quad (12)$$

$$\frac{E_{11}}{E_m} = \frac{(1 + \eta v_f)}{(1 - \eta v_f)} \quad (13)$$

$$\eta = \frac{(E_f/E_m - 1)}{(E_f/E_m + \zeta)} \quad (14)$$

$$\zeta = 2 \left(\frac{1}{d} \right) \quad (15)$$

where $1/d$ is the fiber aspect ratio. Extension of this analysis to consider the case of $v_f \neq v_m$ and an anisotropic discontinuous fiber has not, to the author's knowledge, been made.

Differential fiber-matrix expansion can also lead to matrix cracking or interface cracking, depending on whether the tensile strength of the matrix or the composite transverse tensile strength is lower. The matrix strength in MMC is higher than in resin matrix composites so that interface cracking may be more prevalent. Stresses may be similar nevertheless, for while α_{metal} is $\sim (1/2)\alpha_{\text{resin}}$, the fabrication temperatures of MMC are generally higher. Cooper and Sillwood²¹ equate the tensile load in the matrix with the compressive load in the fibers to derive an expression for the temperature excursion needed to induce failure;

$$\Delta T = \frac{E_o E_m}{E_f V_f (\alpha_m - \alpha_f)} \quad (16)$$

The matrix tensile failure strain is

$$\epsilon_m = \left(\frac{12 \gamma_m \tau E_f V_f^2}{E_o E_m^2 V_m r} \right)^{1/3} \quad (17)$$

where

$$\begin{aligned} \gamma_m &= \text{fracture surface energy} \\ \tau &= \text{frictional stress at interface} \\ r &= \text{fiber radius} \end{aligned} \quad (18)$$

The strain per crack, and, hence, the dimensional change of the composite could, in principle, be estimated by the shear lag theory of Bailey et al.²² Again, these theories must be extended to cover plastic flow in MMC. A preliminary approach to the measurement of microcracking onset temperatures, ΔT , and coefficients of cracking expansion has been made in our laboratory.²³ Neubert²⁰ has applied the same classical lamination theory, modified with a stepwise linear analysis involving E_f , E_m , α_f , and α_m changes with temperature, to prediction of ΔT for a 45 volume percent unidirectional graphite-Mg composite, assuming a matrix failure strength criterion of 48 MPa (7000 psi). His value of $\Delta T = 610$ K suggests that microcracking is to be expected at lower temperatures than are common for graphite-epoxy (180-250K)²³. In addition, the energy release per crack is likely to be less than in the graphite epoxy case, and consequently more sensitive detection may be required.

Additional related factors requiring precise length measurements include edge or end effects, thermomechanical history, and misorientations, especially with very low CTE values. For a unidirectional composite,

$$\alpha_{\theta} = \alpha_0 \cos^2 \theta + \alpha_{90} \sin^2 \theta \quad (19)$$

It can be shown that a deviation of $\theta = 3$ deg between fiber and measurement directions can lead to a 6.5% error in the α_0 of a 45 vol% graphite-Mg composite.

These considerations indicate that a wide variety of theories apply to the thermal cycling behavior of MMC, and verification of these is likely to require highly precise measurement techniques.

III. EXPERIMENTAL TECHNIQUES

Continuous measurement of the relative positions of two points is required for complete knowledge of the linear thermal expansion characteristics of a material. Reflected low-energy laser beams offer independence from shape, size, fabrication, thermal lag, and contact stress effects.²⁴ Furthermore, Michelson interferometry transfers dependence on a reference material to the laser frequency (stabilized in this work on the Lamb dip to one part in 10^9 in 500 hr). When all optics are placed in a vacuum chamber, there are negligible errors as a result of refraction in beam paths, or window or operator effects. All (fringe) information is generated at the beam splitters. The principle of a two-channel Michelson interferometer is shown in Fig. 1.²⁵ The laser beam is split 50/50 at beam splitter (B3) into right and left (sample) side interferometers. Designating the sample ends by S, and mirrors by M, for the right-hand side, the interferometer optical path length difference is

$$\text{OPLD}_1 = \overline{B_1 S_1} - \overline{B_1 M_6} \quad (20)$$

Similarly,

$$\text{OPLD}_2 = \overline{B_2 M_5} - \overline{S_2 M_4} - \overline{B_2 M_4} \quad (21)$$

Now,

$$\Delta \text{OPLD}_2 - \Delta \text{OPLD}_1 = \overline{\Delta B_2 M_5} - \overline{\Delta S_2 M_4} - \overline{\Delta B_2 M_4} + \overline{\Delta B_1 S_1} - \overline{\Delta B_1 M_6} \quad (22)$$

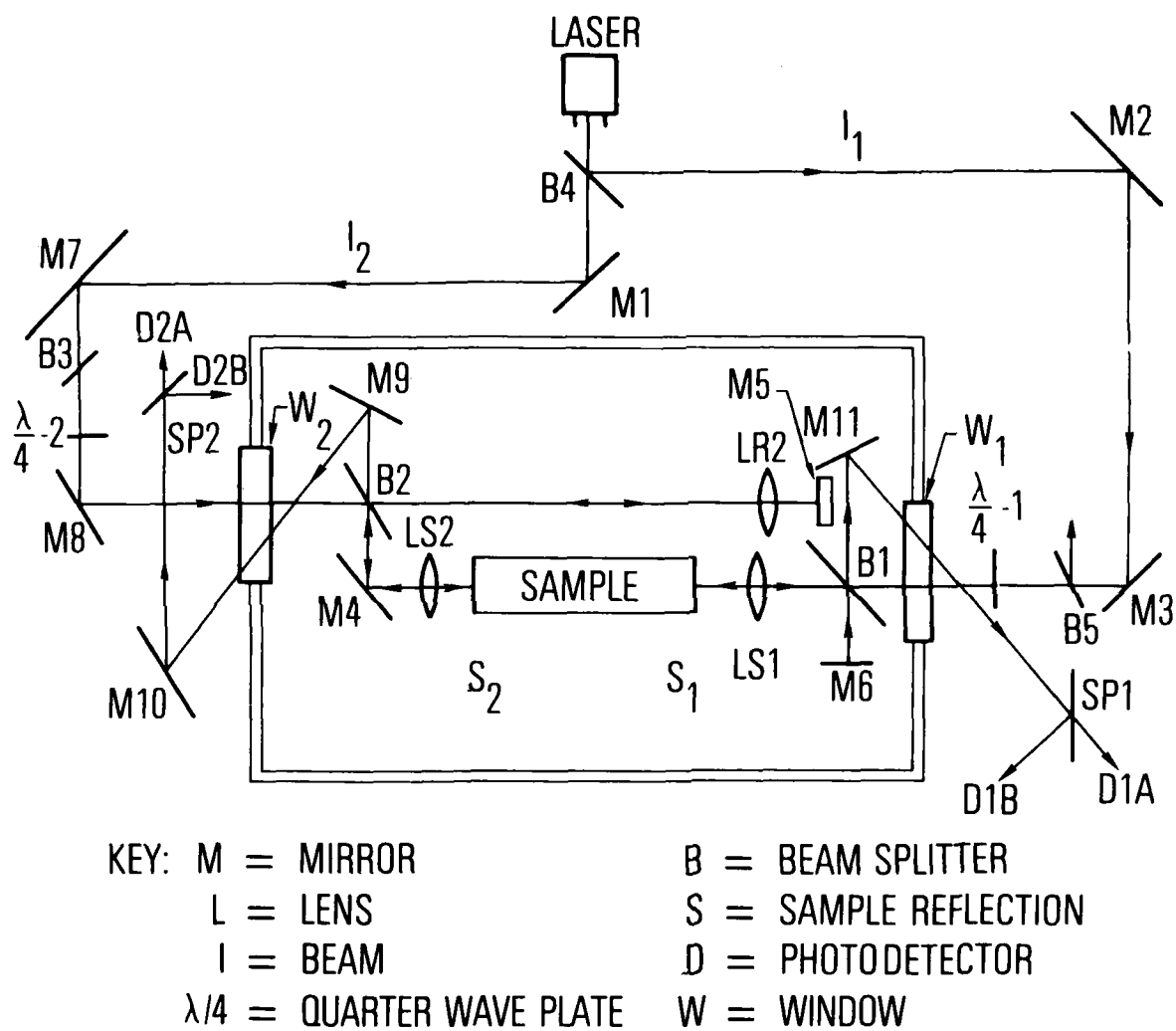


Fig. 1. Two-Channel Michelson Laser Interferometer

Assume

$$\overline{\Delta B_2 M_4} = \overline{\Delta B_1 M_6} \quad (23)$$

$$\overline{\Delta B_1 M_4} = \overline{\Delta B_2 M_5} \quad (24)$$

Note that

$$\overline{\Delta B_1 M_4} = \overline{\Delta S_2 M_4} + \Delta L_s + \overline{\Delta S_1 B_1}$$

where L_s is the sample length

$$\Delta L_s = \Delta OPLD_2 - \Delta OPLD_1 \quad (25)$$

Consequently, the sample length change ΔL_s is merely the difference of the changes in the two OPLDs.

A method of supporting the test sample is shown in Fig. 2. The cross section of the material is arbitrary; the length is limited only by the size of the vacuum chamber (and resultant optics separation) available and by the amount of heat flow the system can tolerate. Thin horizontal Invar or Zerodur support rods have proved highly successful because their low CTEs produce a minimal effect on the sample position in space, and, in addition, their supports are close to room temperature at all times.

The system employed transfers the compensation path B2-M5 in Fig. 1 to a position directly above the M4-sample-B1 path, thus eliminating the effects of transverse temperature gradients in the support plates (Fig. 2). Test samples for metal matrix composites were generally polished at the ends to an rms finish

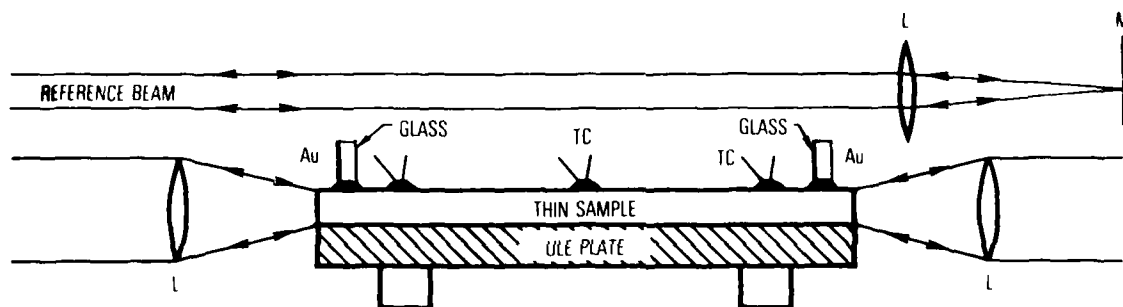


Fig. 2. Thin Test Sample Inside Two-Channel Michelson Interferometer. Aluminized end faces, polished $< \lambda/5$, are preferable to alternate mounted mirrors

of $\lambda/2$ to $\lambda/5$ and coated with a few hundred angstroms of vapor-deposited Al. Au or Cr films, useful for ceramic samples, were found to be less successful on high graphite fiber end surfaces.

The accuracy of these measurements, in principle a measure of their traceability to a standard, is sensitive to thermal gradients in the system and sample end-face geometry. The former errors are roughly proportional to the sample temperature excursion, so that the total strain values are more accurate at 300 K than at 100 or 500 K. The sum of all errors for a 250 K excursion is about 5×10^{-8} m. An average CTE measurement on a 10^{-1} m sample implies an rms error σ_{CTE} of $1.2 \times 10^{-9} \text{ K}^{-1}$.

The four photodetector signals can be digitally processed to count automatically in steps of $\lambda/8$ (7.9×10^{-8} m). The analog output of a photodetector for each sample side can be amplified and continuously recorded (Fig. 3). The vibration of the system represents a noise level on the order of ± 0.1 V in a 4-V signal, which, in turn, represents a length resolution on the order of $\lambda/160$ or 4×10^{-9} m. Fringe interpolation to comparable resolution can also be made with an xy to θ converter. The error in ΔT measurement is 0.7 K since it depends on the difference of two temperatures with thermocouples (Cu-constantan) where absolute accuracy is only about ± 0.5 K.

A comparable system to handle larger samples is described in Reference 25. Here, phase modulation techniques are employed for the signal processing. By oscillating the reference mirror, the intensities of the even and odd harmonics received by a single photodetector are 90 deg out of phase. Again, quadrature signals are needed to measure the direction of the fringe motion. Length changes as low as 10^{-12} m have been detected in our laboratory by this method, but resolution is generally limited by mechanical vibration of the optics system, e.g., as induced by the flow of liquid nitrogen for cooling. This technique has been used to measure the CTE of individual precursor wires (and could also be used for a single graphite filament). How a 201 Al alloy with 40% T50 fibers (0.68 mm) diameter wire of gage length 0.292 m was tested is shown in Fig. 4. (The CTE from -40 to 80°C averaged $1.72 \pm 0.01 \times 10^{-6} \text{ K}^{-1}$.) The lateral constraint on the lower mirror is introduced to inhibit

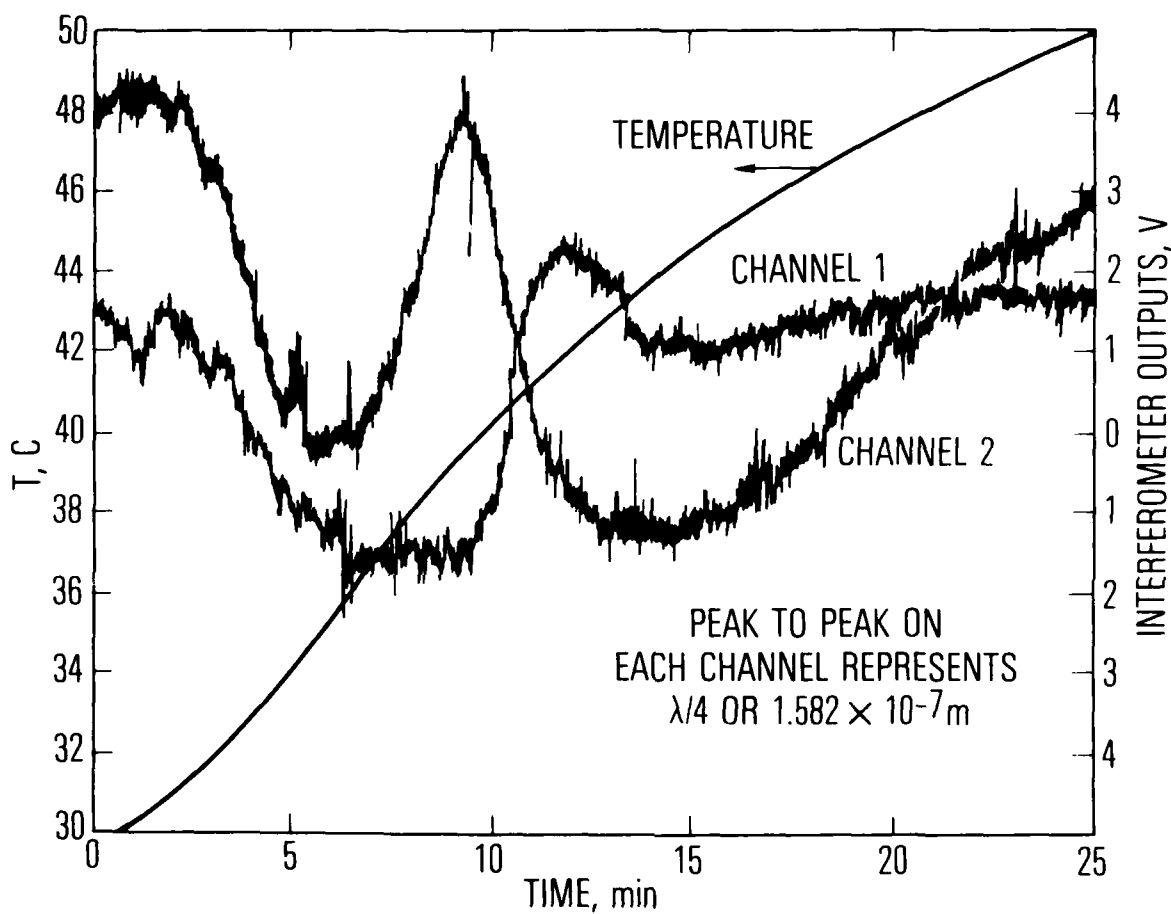


Fig. 3. Typical Photodetector Output from Two-Channel Michelson Interferometer. Two photodetectors per channel are used to determine direction of sample end-face movement.

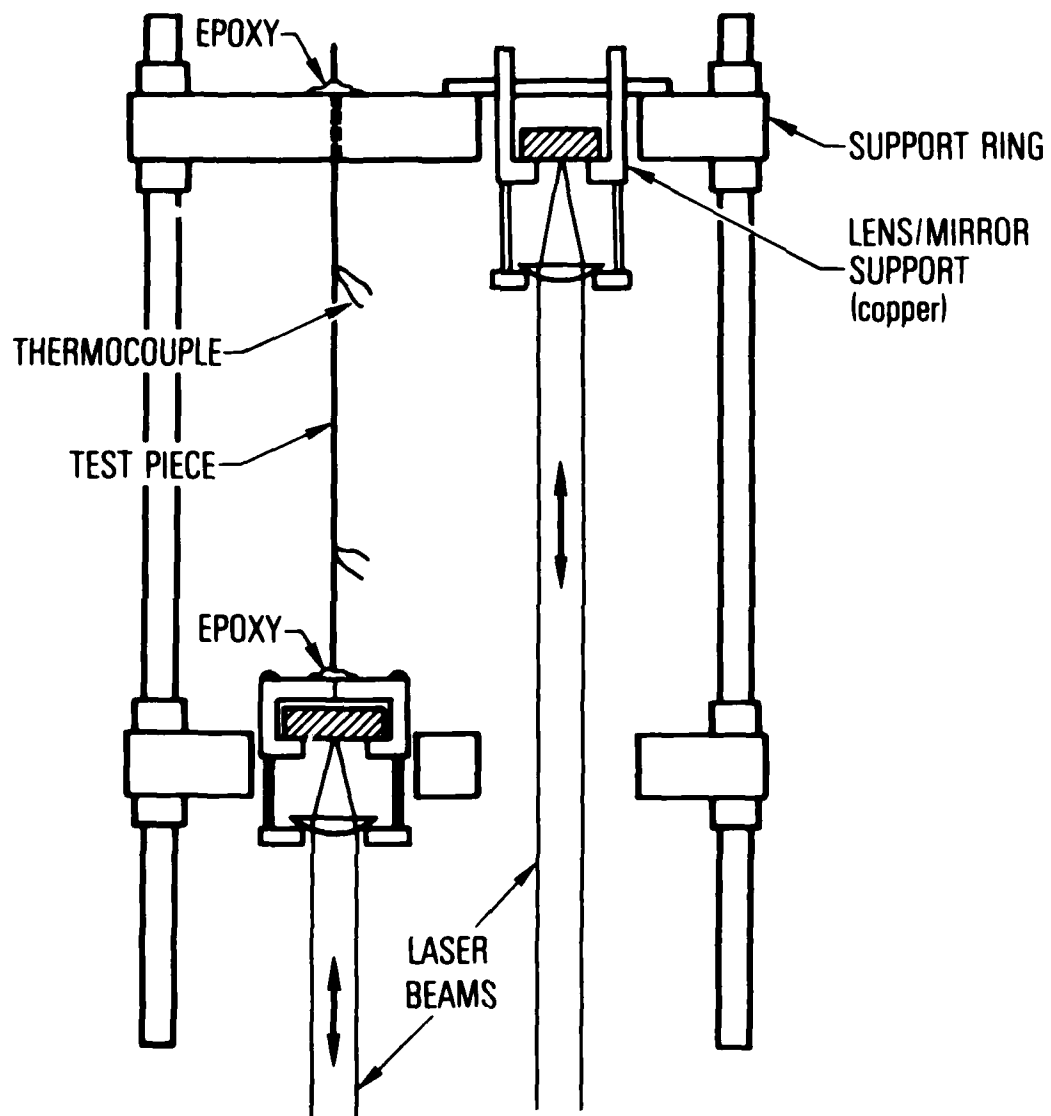


Fig. 4. Apparatus for Thermal Expansion Testing of Thin Wires, Plates, or Fibers

pendulum motions at about 0.9 to 1 Hz. Forced harmonic oscillations occurred in the 5 to 10 Hz range, but, whether present or inhibited, they do not preclude CTE signal processing.

A recent development²³ involves the simultaneous recording of high-frequency signals (0 to 25 kHz) received by the photodetectors during low-temperature CTE measurements.

Microcracking at low temperatures causes pulses that have a high dc content, which decreases as $\exp(-f^2)$. The resultant stress waves cause length changes that are readily detectable, since attenuation is lowest at the lowest frequencies. Conventional acoustic emission, besides requiring transducers, operates mainly at frequencies of 150 kHz and above. The apparatus used to detect, store, and analyze microcracking information is shown schematically in Fig. 5. A separate signal proportional to the temperature is converted to a frequency, giving spectrum analysis continuous built-in temperature information. In addition to microcracking and liquid nitrogen-induced vibrations, the opto-acoustic system detects sample sliding, e.g., on the ULE support plate (Fig. 2) and optic system vibrations. A computing spectrum analyzer permits a microcracking or other high-spectral-content event to trigger a frequency spectrum that can be added, subtracted, or divided by another spectrum chosen at will during the experiment. Figure 6 represents a ratio of high-to-low liquid nitrogen flow rates during cooling, at 230 K with a graphite-Mg sample. Characteristic frequencies relate to system resonant frequencies. (In this case, the sample resonant frequency was ~ 83 kHz, so microcracking would be identifiable mainly from pulse analysis.) Thin quartz transducers can also be attached for the ultrasonic measurement of sound velocity.²⁶ The time to traverse a 1.6-mm-thick graphite-Mg sample (Fig. 2) is on the order of 0.45 μsec . This time can be measured continuously to an accuracy of $\pm 0.01 \mu\text{sec}$. Since

$$E_c \sim \frac{\rho l^2}{gt^2} \quad (26)$$

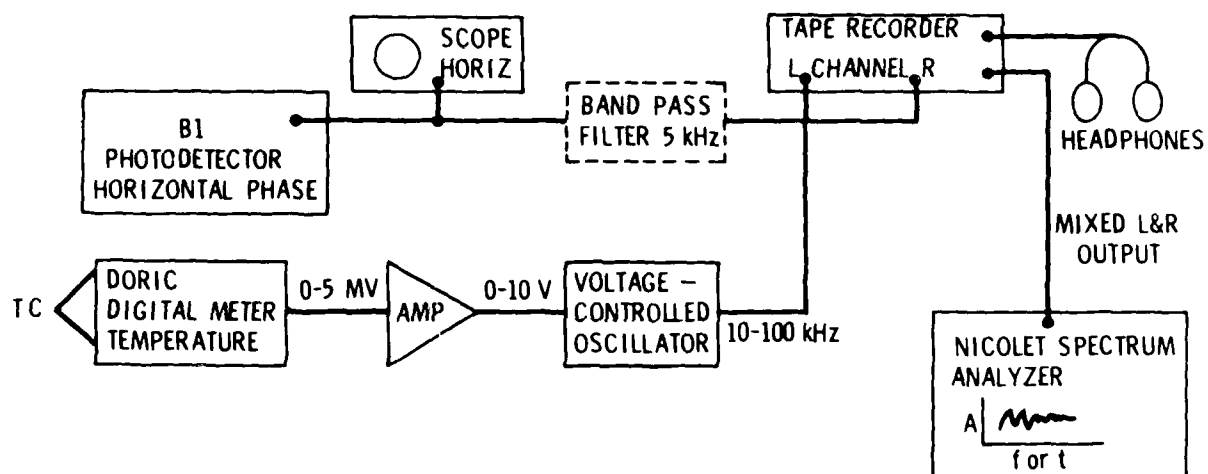


Fig. 5. Opto-acoustic Recording and Analysis of Microcracking

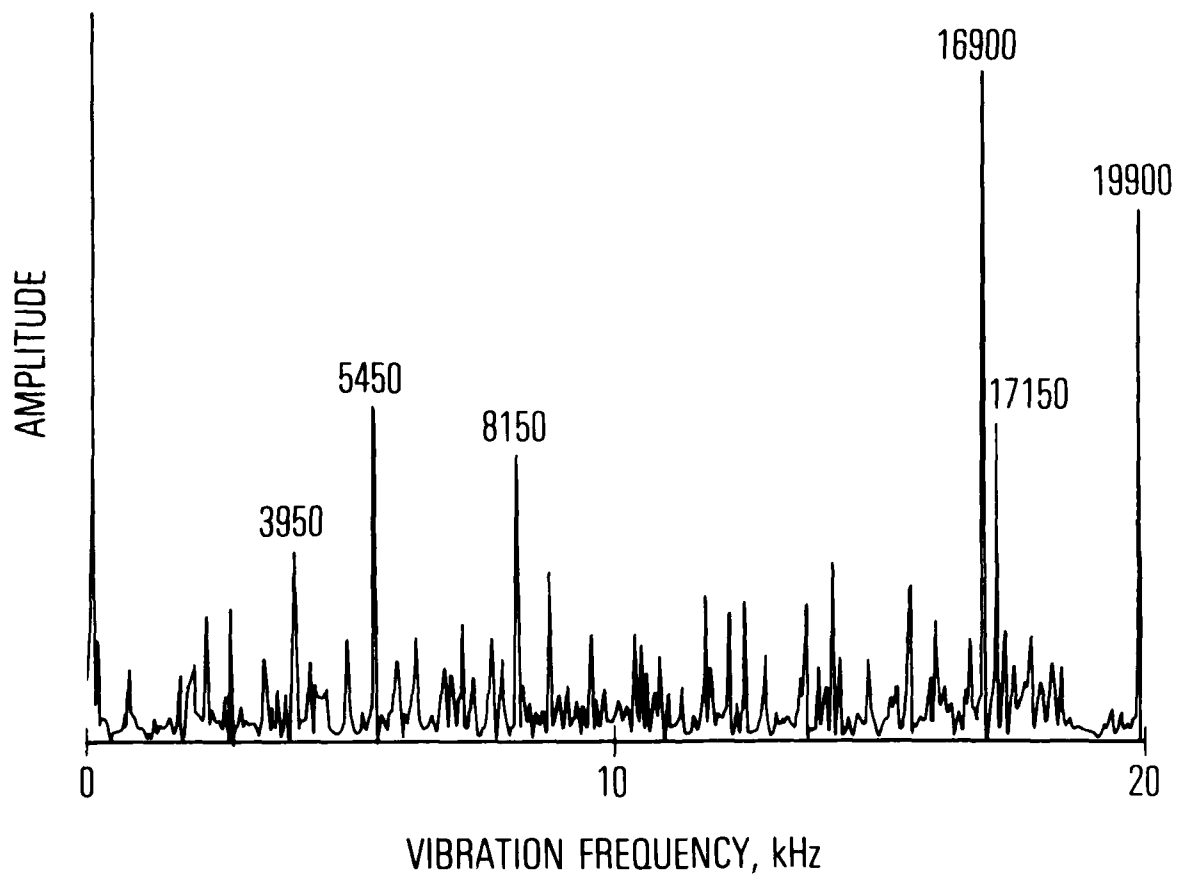


Fig. 6. Amplitude Versus Frequency from Sample End Vibrations.
Trace is ratio of high-to-low liquid nitrogen flow
(vibration-inducing) during sample cooling.

where ρ is the sample density, g the acceleration caused by gravity, and l the distance traveled, a continuous measurement of E on the order of ± 0.98 GPa, or one part in 23 is possible. This would enable changes in the (transverse) stiffness to be continuously correlated with temperature, CTE, and microcracking behavior. Comparative pulse analysis for each interferometer (Fig. 1) could, in principle, provide simultaneous monitoring of E .

IV. RESULTS

A. GRAPHITE-AL

In early studies carried out with Thornel T50 fibers, CTE values at 300 K of up to 1-1/2 times that expected from a prediction based on Eq. (1) were obtained. (Use of Eq. (1) is a convenience, as it tends to separate out fabrication effects from plastic flow effects during CTE measurements.) These data could be correlated with composite elastic modulus, especially in the transverse direction. Poor fiber matrix bonding is readily apparent in transverse stress-strain testing, while fiber degradation resulting from processing is reflected by longitudinal modulus values below those predictable by a rule of mixtures. Samples with the highest E_o values had CTEs close to the $\overline{E\alpha}/\overline{E}$ curve predicted from initial constituent properties (Fig. 7). Higher temperature data (to 67° K) were obtained for both α_o and α_{90} for a 28 vol% T50/201 sample. (A linear variable differential transformer with CERVIT push rods was used, as well as the laser interferometer.) The data are shown in Fig. 8. The longitudinal CTE (α_o) agreed well with predictions based on $\overline{E\alpha}/\overline{E}$ when the change in E_{A1} with temperature was taken into account. T50 fibers approach near-zero CTE while the E_{A1} values drop steeply in the region 550 to 650 K. These factors combine to yield a very low α_o value for this composite in the 450 to 700 K temperature range. The transverse CTE values were found to slightly exceed those of pure aluminum. Positive deviations from a rule-of-mixtures CTE can be expected.^{7,10} Figures 9 and 10 show Fizeau interferometer data of the effect of prestraining on thermal cycling behavior. These results also depend on heating/cooling rates.

The GY70/201 results for the temperature range 295 to 350 K fell close to those predictable by an $\overline{E\alpha}/\overline{E}$ relationship (Fig. 7). In addition, there was no hysteresis in successive heating-cooling cycles. A ± 17 -deg angle-ply layup measured in the 0-deg direction did show slight hysteresis - the cooling curve consistently fell about 10 to 15 $\mu\text{m/m}$ higher than the heating curve at the same temperature for the three cycles measured. Agreement with an Eq. (19) prediction is good if the value of α_{11} is based on the bulk modulus $\overline{K\alpha}/\overline{K}$; i.e., $\alpha_{11} = 8.6 \times 10^{-6} \text{ K}^{-1}$ (Fig. 7) and α_{22} is taken as $25 \times 10^{-6} \text{ K}^{-1}$.

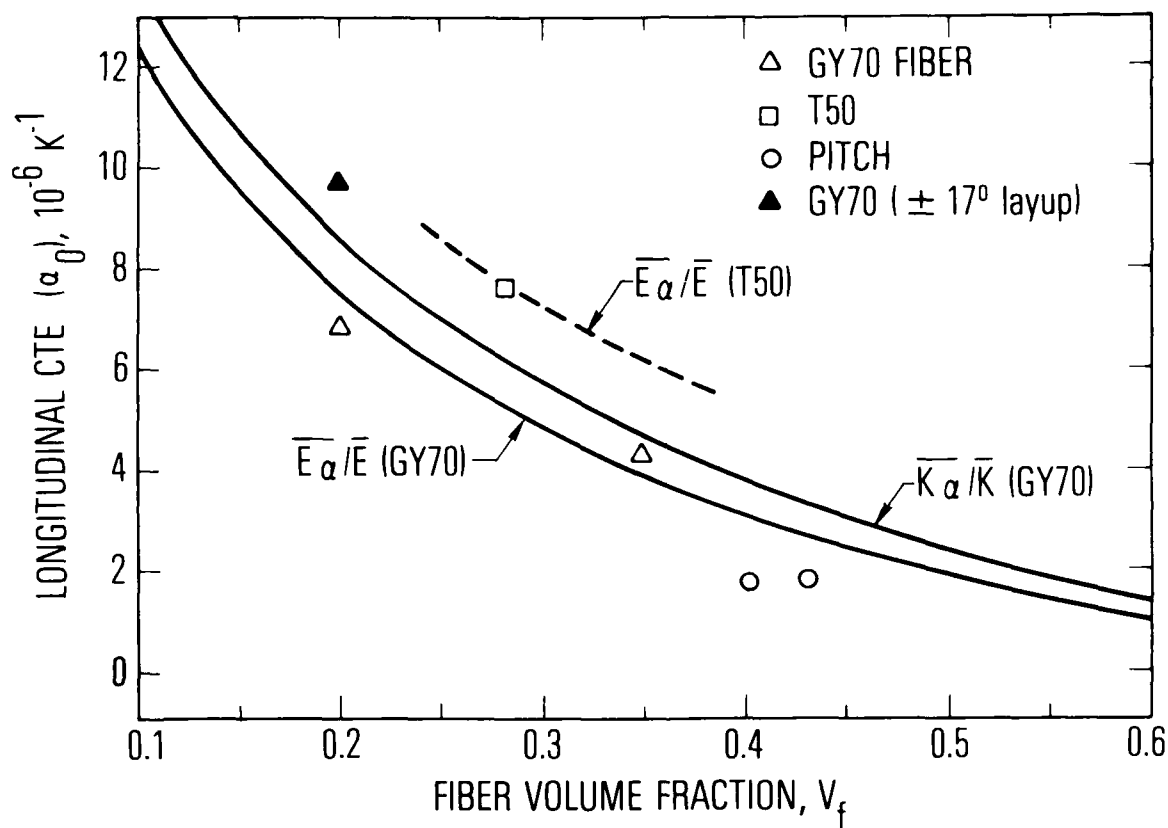


Fig. 7. CTE Data at 300 K for Unidirectional Graphite-Al Samples Compared with Predictions Based on Eq. (1) and Table 2. Pitch refers to Pitch 55, but the modulus of these early fibers was not separately determined and may have been somewhat higher than 55×10^6 psi.

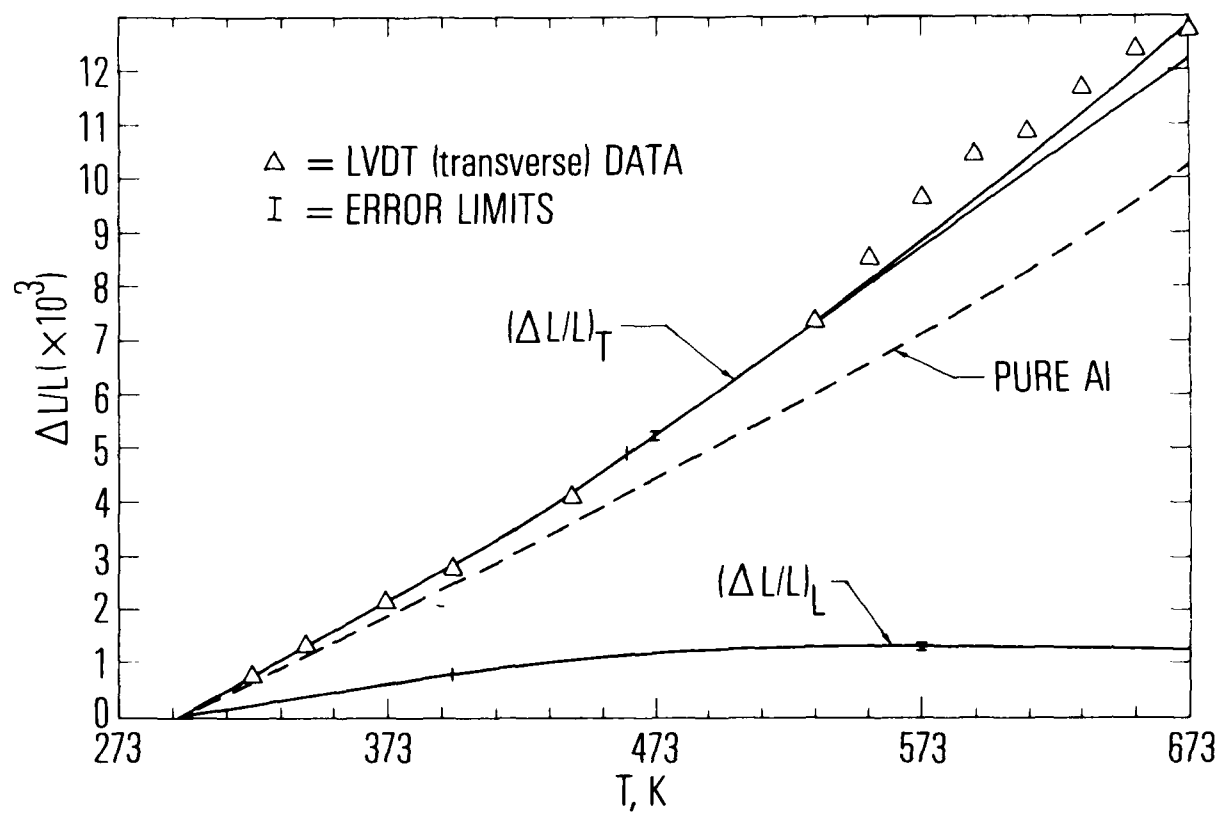


Fig. 8. Transverse and Longitudinal Expansion Data for Graphite-Al Composites

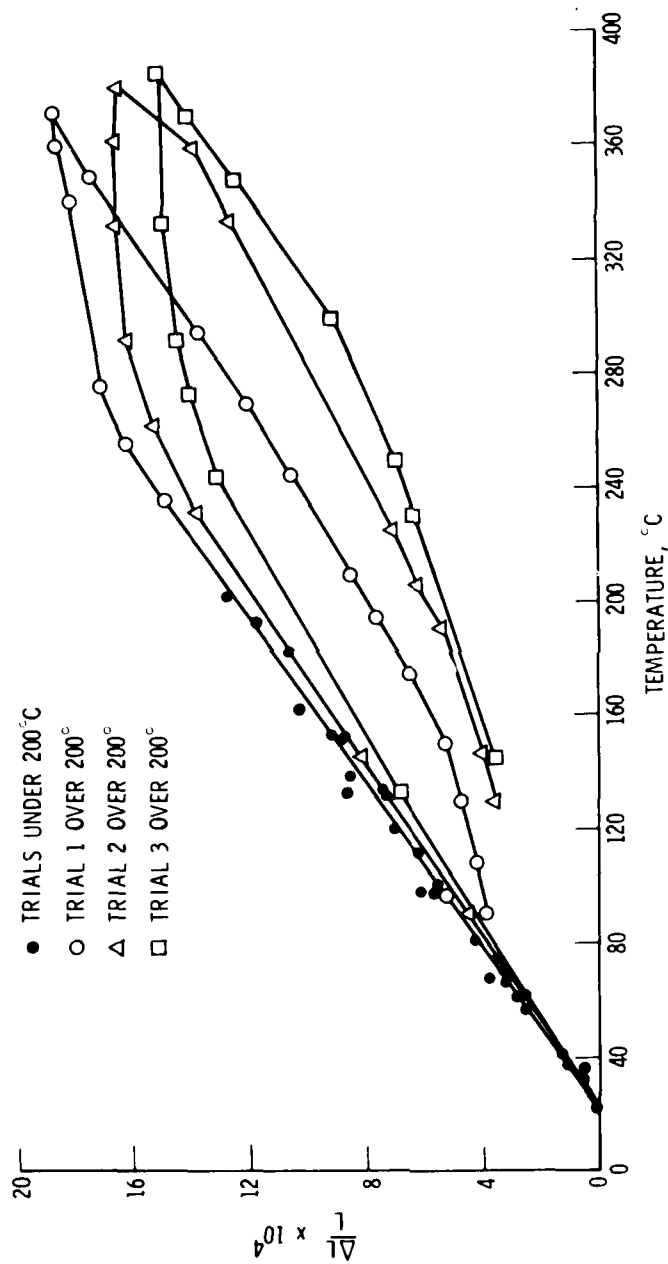


Fig. 9. Thermal Cycling Behavior of Unstrained Unidirectional T50/202 Al Composite in the Fiber Direction. Heating rate averaged 9°C/min to 400°C and ~2°C/min back to 25°C.

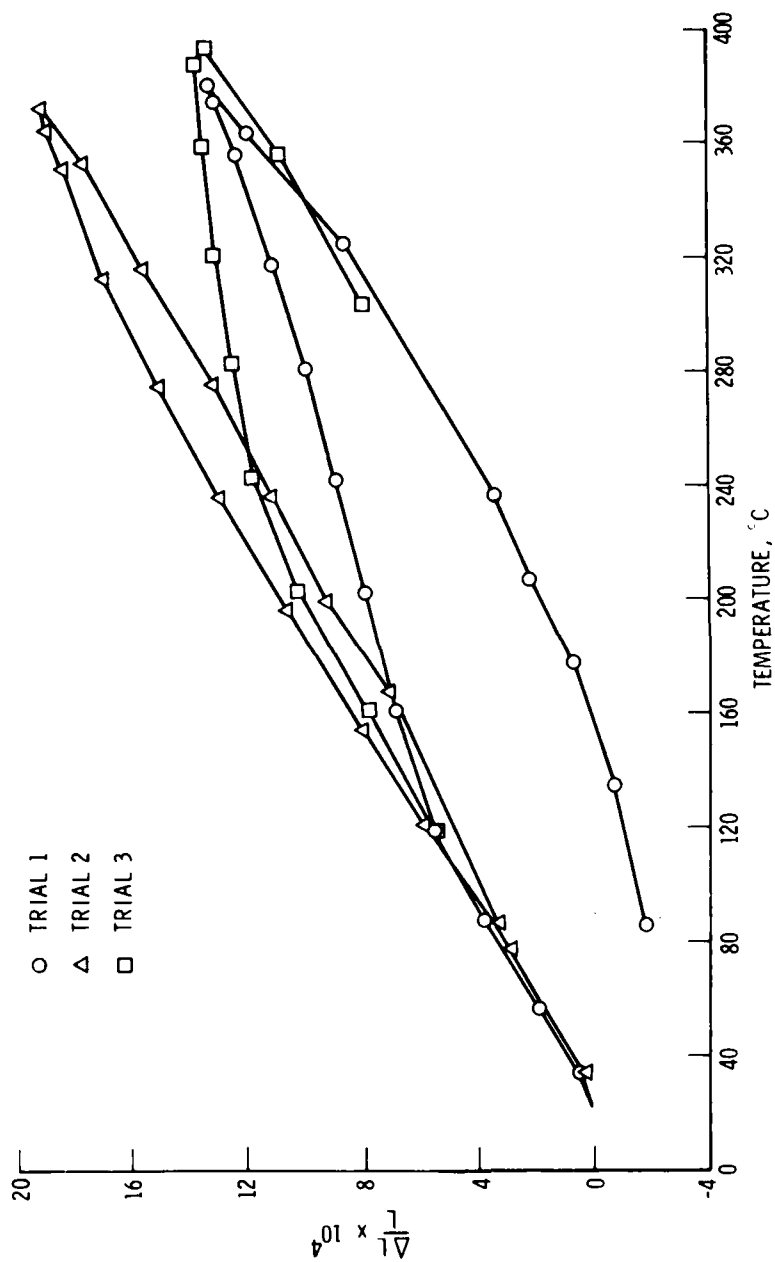


Fig. 10. Thermal Cycling Behavior for Unidirectional T50/202 Al Prestrained to Its Secondary Modulus (48 ksi) in the Fiber Direction. Heating rate 9°C/min to 400°C and 2°C/min back to 25°C.

The former requirement suggests dependence on Poisson's ratio effects in MMC angle-ply composites. The elastic modulus E_o for these composites followed a rule of mixtures, confirming the value of E_f used in the calculations.

The most recent data were obtained with VS0054 pitch fibers (Union Carbide) in a 6061 alloy. These fibers have shown E_f values in the range of 586 to 760 GPa. Mechanical test data indicate that $E_f \sim 690$ GPa in the sample tested here. The room-temperature CTE values fell predictably below the curves in Fig. 1 because of the increased value of E_f over GY70. Below 230 K, some evidence of microcracking was found in the form of a positive deviation from the high-temperature $\Delta L/L$ versus T behavior.

B. GRAPHITE-Mg

It can be shown that the transverse CTE (α_{90}) is relatively insensitive to E_f and α_f , so that the α_o values are of primary interest here. Some α_o data at 300 K, obtained for a variety of samples employing different fibers, are shown in Fig. 11. In this case, the curves based on Eq. (1) utilize pitch fiber properties (Table 1). As in the graphite-Al case, the lower V_f samples are also the earlier ones, where nonoptimum fabrication procedures tended to result in reduced values of E_f . The data for the GY70 and T50 fiber samples would be expected to lie higher than a $\overline{E\alpha/E}$ prediction based on VS0054 pitch fibers. Whereas the room temperature CTE values are generally as expected, the low-temperature behavior is more complex. Data for graphite pitch fiber composites on successive cooling-heating cycles are given in Table 2 and Figs. 12 through 16. One difference appears to be caused by microstructures. The $V_f = 0.504$ and 0.45 samples were hot pressed, consisting of three layers or three plies of previously fabricated material; the $V_f = 0.436$ consisted of only one layer. In the latter sample, there was negligible positive deviation in $\Delta L/L$ on the first cooling cycle; in the others, the slope is initially closer to a zero CTE. This approaches the high-temperature CTE after a number of cycles to low temperatures (about four in the case of $V_f = 0.45$ sample). In addition, this sample (Fig. 14) showed discontinuous "bumps" in the curve that progressed to lower temperatures on repeated cycling. This phenomenon is not yet explained. Cycling rates were about

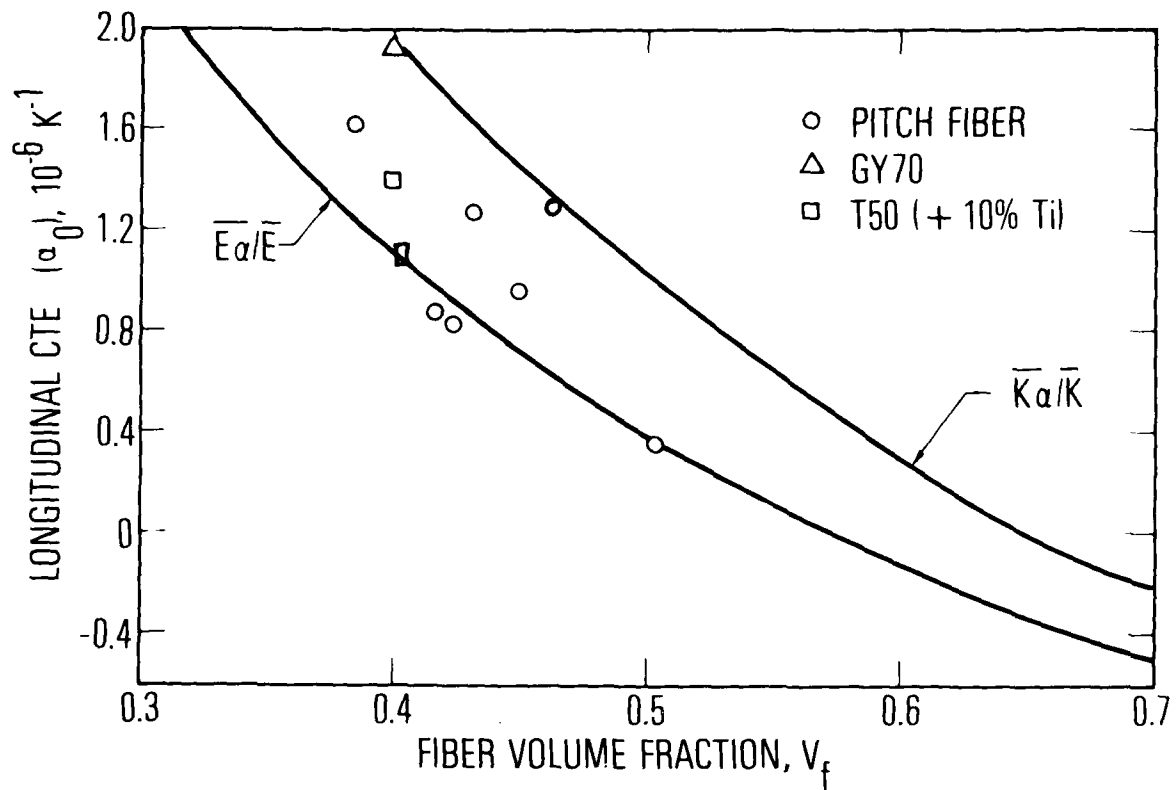


Fig. 11. CTE Data at 300 K for Unidirectional Graphite-Al Samples Compared with Predictions Based on Eq. (1) and Table 2 (VS0054 Pitch Fibers)

Table 1. Summary of Results of CTE Measurements on Graphite-Mg^{a,b}

Sample No.	Fiber	Matrix	Surface Foil	No. of Layers	V _f	L _o (in.)	$\bar{\alpha}_{11}$ Near RT
242-TEL-LMSC	VS0054	AZ91C	AZ61A	1	0.436	2.94	$1.27 \times 10^{-6} \text{ K}^{-1}$ ($0.706 \times 10^{-6} \text{ }^{\circ}\text{F}^{-1}$)
243-TEL-LMSC	VS0054	AZ91C	AZ61A	3	0.504	2.96	$0.34 \times 10^{-6} \text{ K}^{-1}$ ($0.189 \times 10^{-6} \text{ }^{\circ}\text{F}^{-1}$)
282-B-TEL-1	VS0054	AZ91C	AZ61A	1	0.381	2.97	$1.626 \times 10^{-6} \text{ K}^{-1}$ ($0.903 \times 10^{-6} \text{ }^{\circ}\text{F}^{-1}$)
283-B-TEL-1	VS0054	AZ91C	AZ61A	3	0.45	2.96	$0.96 \times 10^{-6} \text{ K}^{-1}$ ($0.53 \times 10^{-6} \text{ }^{\circ}\text{F}^{-1}$)

^aAll samples are hot pressed at 875°F, and quenched in liquid nitrogen three times prior to test. Unidirectional.

^bAll samples are 0.25 in. wide. Samples 242 and 282 are 0.023 in. thick, 243 is 0.07 in., 283 is 0.064 in.

Table 2. Some Properties of Composites Related to CTE

Property	Composite				
	B-Al	Graphite-Al	SiC-Al	Graphite-Mg	Graphite-Epoxy
Fiber	"Borsic"	GY 70	"Silag"	VS0054	GY 70
Matrix	6061	201	6061	AZ91C	934
$\alpha_f, 10^{-6} \text{ K}^{-1}$	4.9	-1.1	(4)	-1.2	-1.1
$\alpha_m, 10^{-6} \text{ K}^{-1}$	24	24	24	24.8	51
$E_f, \text{ GPa}$	400	515	(470)	689	530
$E_m, \text{ GPa}$	68	68	68	45	3
ν_f	0.2	0.2	0.2	0.2	0.2
ν_m	0.25	0.25	0.25	0.291	0.382
$E_{11}, \text{ GPa}$	220	200	100	300	300
$E_{22}, \text{ GPa}$	145	36	100	34	6.7
$G_{12}, \text{ GPa}$	66	48	60	48	4.9
ν_{12}	0.24	0.29	0.27	0.28	0.192
$F_T^{tu}, \text{ MPa}$	120	50	100	50	27
$\alpha_1^c, 10^{-6} \text{ K}^{-1}$	8.7	4	13	1	-1.0
$\alpha_2^c, 10^{-6} \text{ K}^{-1}$	15.3	18	24	21	26
V_f (Assumed)	0.5	0.35	0.2	0.45	0.62
l/d	∞	∞	75	∞	∞

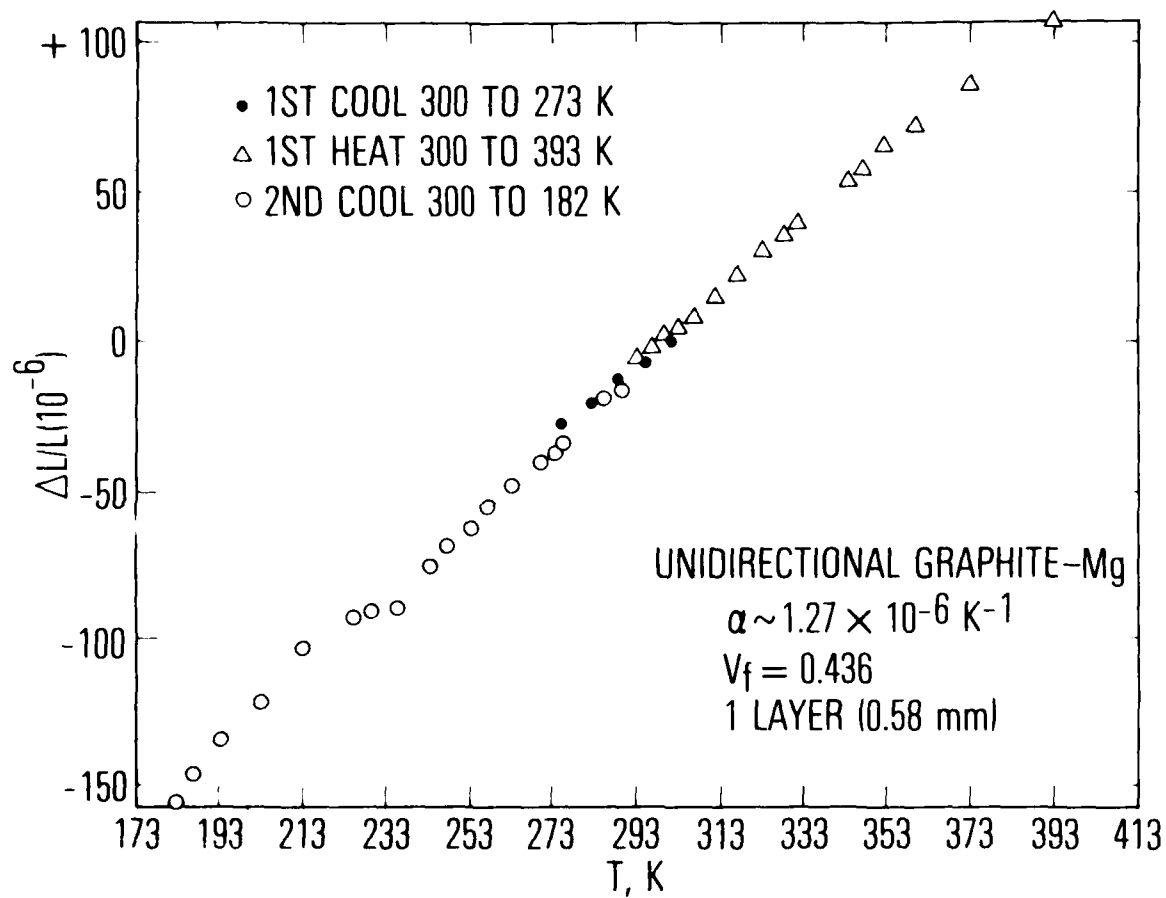


Fig. 12. CTE Data for Unidirectional VS0054-Mg Composite of One-Ply Layer

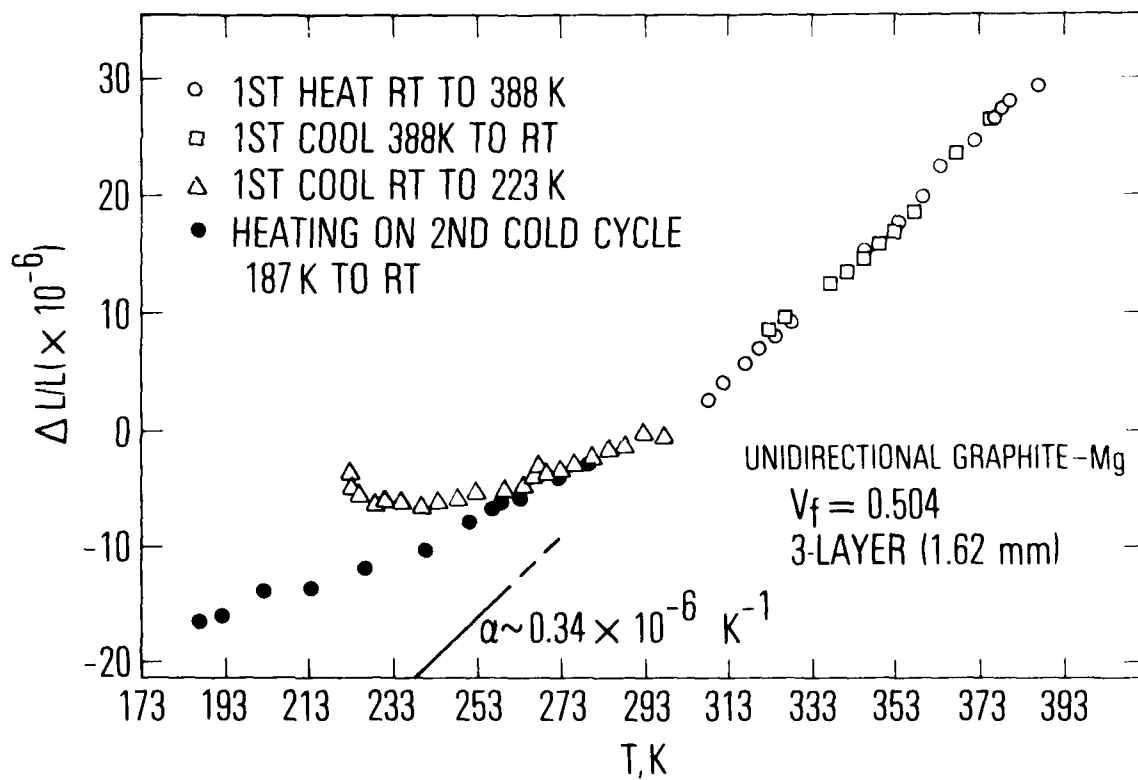


Fig. 13. CTE Data for Unidirectional 50.4% VS0054-Mg Composite of Three-Ply Layers

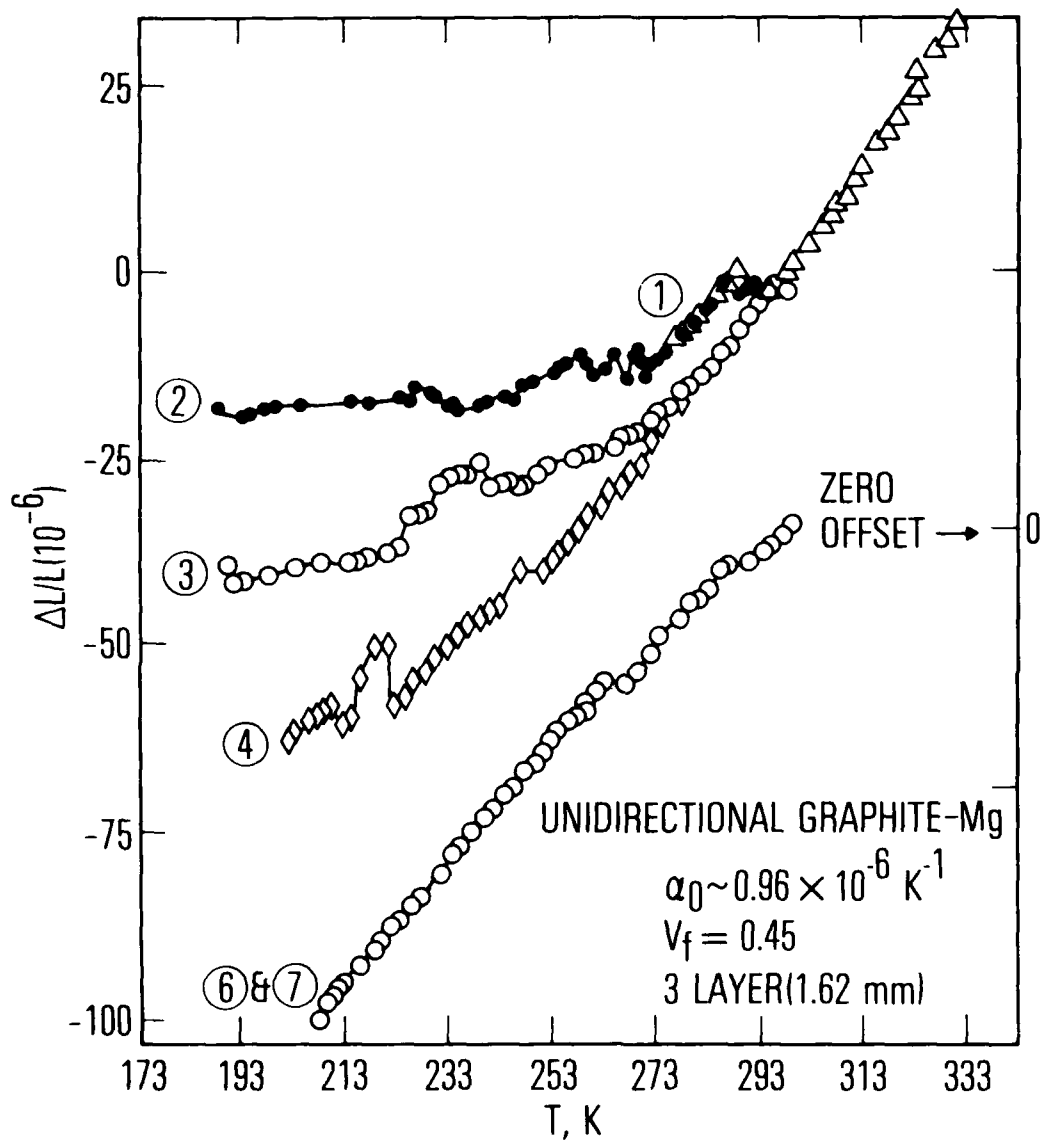


Fig. 14. CTE Data for Unidirectional 45% VS0054-Mg Composite of Three-Ply Layers

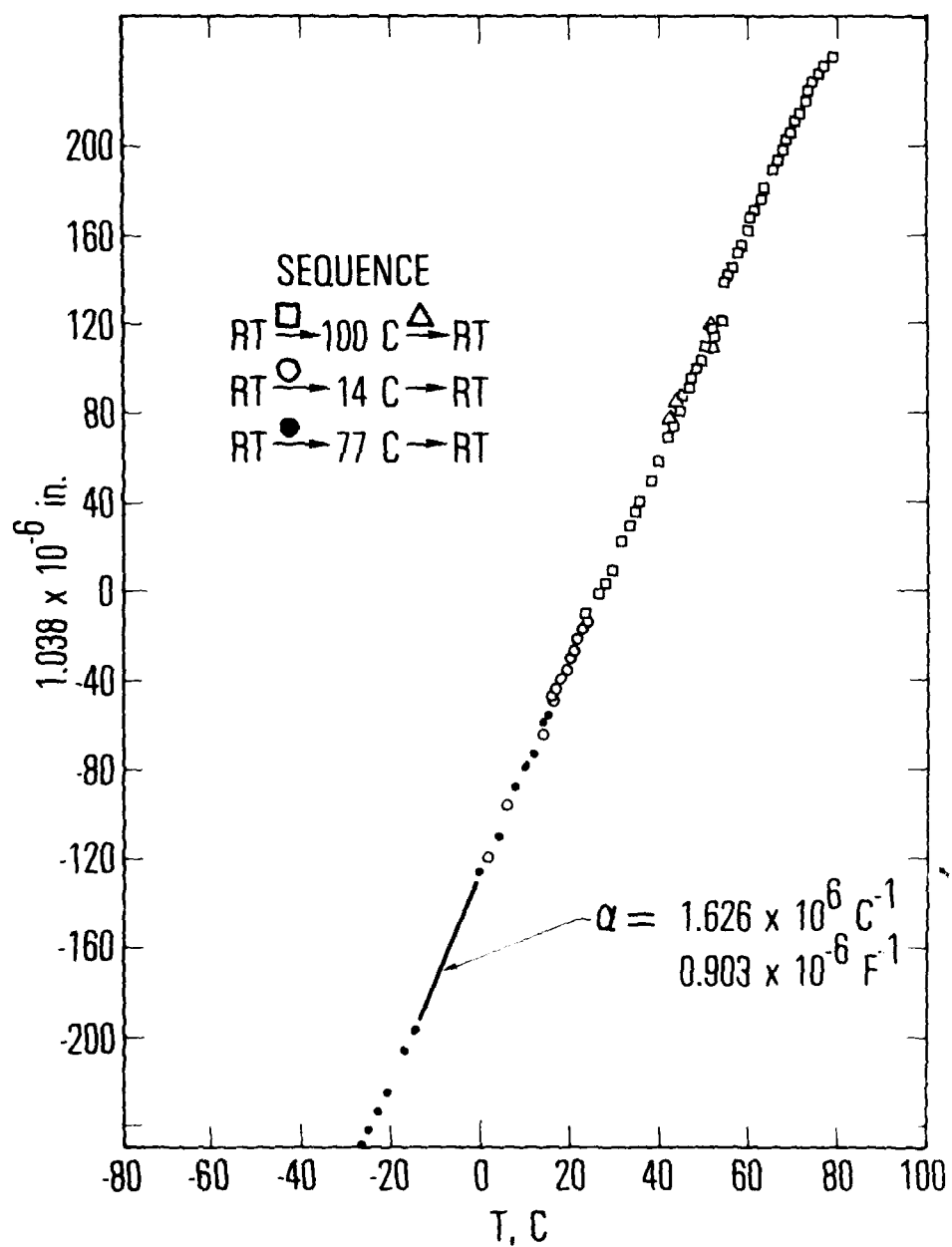


Fig. 15. CTE Data for Unidirectional 38.1% VS0054-Mg Composite of One Layer. (See Table 2.)

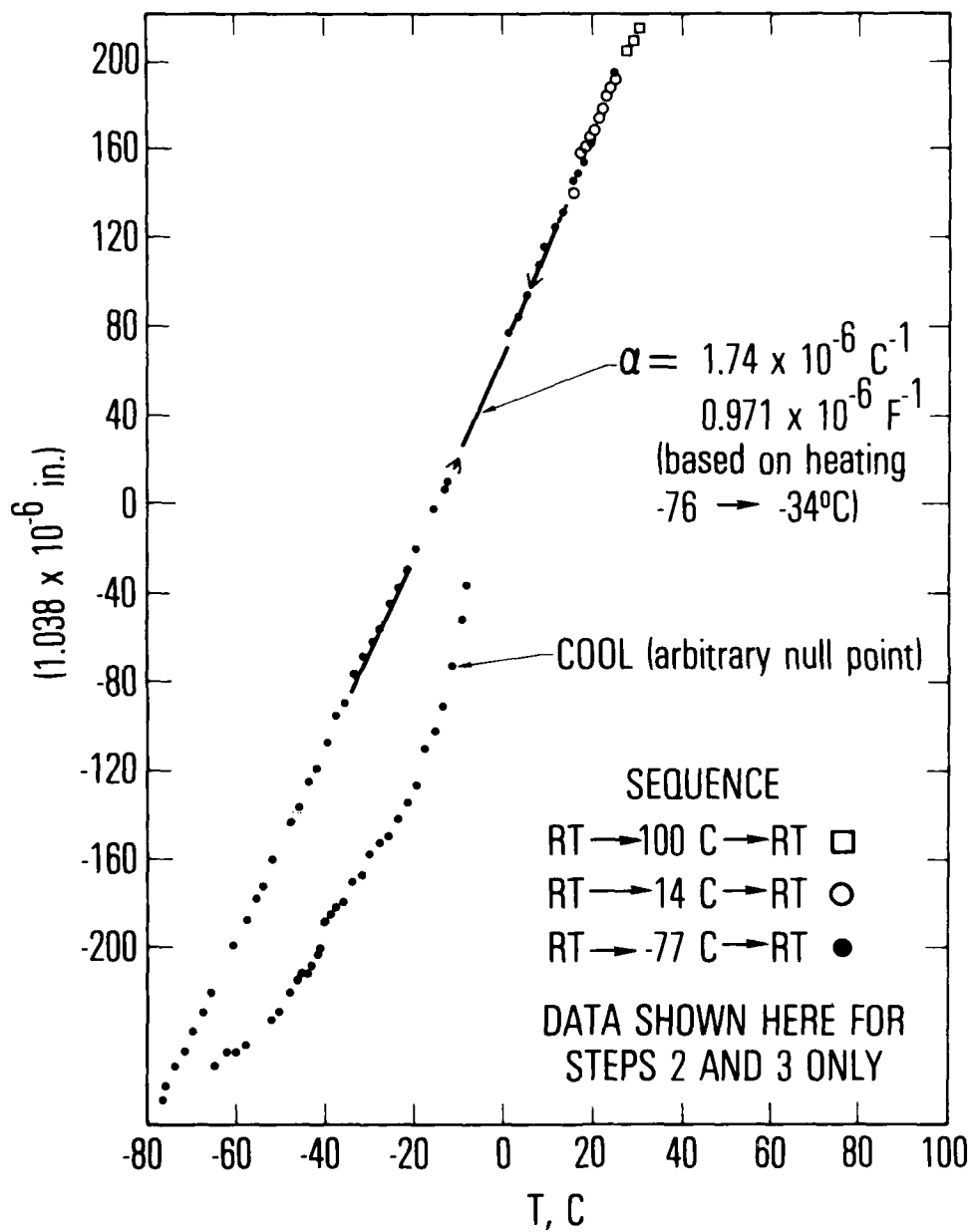


Fig. 16. CTE Data for Sample in Fig. 13 at Lower Temperatures

0.5 - 1°C/min between 0 to -60°C whereas heating rates for -80°C to 0°C were about 1°C/min. These three samples had been prior quenched in liquid nitrogen three times before testing. The reason was that in the graphite-Al case, but not subsequently found for graphite-Mg, the "knee" in the σ - ϵ curve is thereby shifted to higher stress and strain values. Opto-acoustic emission studies have not detected recognizable microcracking down to 200 K. This may be partly because of the plasticity of Mg at low temperatures and partly because the small samples used have longitudinal resonant frequencies above the sensitivity range for the tape recorder. Delamination effects, or the effect of a purely Mg interlayer between the plies must also be considered.

Kural and Ellison²⁷ indicate that thermal expansion measurement errors can arise as a result of end distortions and thermal flexure of asymmetrical specimens. Their results for GY 70/Al suggest that the error for a 3-in.-long sample with a straight end for $T < \text{room temperature}$ is on the order of 0.7%, and for $T > \text{room temperature}$ in the region 2 to 3%. These errors are possible with the present results, except that they did not necessarily occur (as they would have with a dilatometer probe). Since the laser beams are focussed to a diameter less than the sample thickness (23 mil), this spot was randomly chosen along the width of the sample (0.25 in.) for maximum reflectivity. Consequently, there was a chance that the reflection point occurs part way between the high and low points of the surface ends.

The bowing error caused by the axial asymmetry of a thin sample increases with sample length and temperature excursion. The sample cannot bow much in a Michelson interferometer, because of rapid loss of reflected beams coincidence, necessary to obtain a fringe pattern; conversely, a lens is always used to permit some sample end-face rotation. A mirror-lens combination helps to ensure that the reflected beam remains parallel to the incident beam. Although there was no consistent trend in the present results explainable by a bowing mechanism (e.g., an S-shaped $\Delta L/L$ versus T curve instead of a straight line), this possible error will be examined quantitatively in the future.

C. SILICON CARBIDE-AL

Preliminary CTE measurements were carried out on SiC whisker reinforced 6061 Al. The whiskers, a commercial product of EXXON,²⁸ have l/d ratios of 75 to 100 with 0.2 to 1- μ m diameters. X-ray diffraction indicates that they are β -SiC with some stacking faults. Fabrication and mechanical properties have recently been discussed by Sarker,²⁸ Skibo,²⁹ and coworkers. Samples with $l_o = 0.0182$ m and 20 wt% randomly oriented whiskers were tested in a quartz dilatometer. Mean α_o values were $13.5 \times 10^{-6} \text{ K}^{-1}$ (293 to 393 K), $15.5 \times 10^{-6} \text{ K}^{-1}$ (293 to 493 K), and $17.5 \times 10^{-6} \text{ K}^{-1}$ (293 to 593 K), with an uncertainty of $\pm 0.2 \times 10^{-6} \text{ K}^{-1}$. Use of Halpin's equations, Eqs. (10) through (15), with the estimated data of Table 1 suggests an oriented discontinuous SiC fiber-Al composite would have α_o values closer to that of pure Al. Further theoretical investigation is required.

V. SUMMARY

Metal matrix composites represent a new class of dimensionally stable composites. Exploration of the theories relevant to thermal cycling behavior suggests that there is still work to be done to account for simultaneous effects of unequal Poisson's ratios, anisotropic fibers, plastic deformation of the matrix, and microcracking. Verification of such theories will require highly precise, continuously recording laser interferometer dilatometers. The requirements and use of such devices, shown to be able to measure strain changes of less than 10^{-9} m/m have been discussed. Extension of these techniques to the simultaneous recording of microcracking or other microstructural changes such as delamination and plastic flow were outlined. Some data on B-Al, graphite-Al, graphite-Mg, and SiC-Al were presented to illustrate the range of thermal cycling behavior that may be obtained. Future work will include testing of recently fabricated B_4C -coated B, SiC-coated B, and continuous SiC fibers in Ti-6Al-4V matrices--systems for which few data are yet available.

REFERENCES

1. Nakamura, H. H. and Larsen, D. C., "Thermal Expansion Behavior of Boron/Aluminum and Bor SiC/Titanium Advanced Composite Materials," presented Fall Meeting American Ceramic Society, Bedford, Penn., 23 October 1974.
2. Ferte, J. P. and Villamayor, M., "Dilatation des Materiaux Composite Bore-Aluminum," Fibre Science and Technology 4, 49 (1971).
3. Ferte, J. P., "La Dilatation Thermique des Materiaux Composites a Matrice Metallique-Analyse Experimentale et Interpretation Theorique," Ph. D. Thesis, University Claude Bernard, Lyon, 21 June 1974.
4. Wright, M. A., "The Effect of Thermal Cycling on the Mechanical Properties of Various Aluminum Alloys Reinforced with Unidirectional Boron Fibers," Metal Trans. 6A, 129-174 (1975).
5. White, M. K. and Wright, M. A., "Investigations into the Mechanics of Thermal Cycling Damage in Metal Matrix Composites," Contract No. N0014-75-C-0352, University of Tennessee Space Institute, Tullahoma, Tenn. (January 1977).
6. Chawla, K. K., "Thermal Fatigue Damage in Borsic Al(6061) Composites," J. Mat. Sci. 11, 1567-1569 (1976).
7. Kreider, K. G. and Patarini, V. M., "Thermal Expansion of Boron-Fiber-Aluminum Composites," Met. Trans. 1, 3431-3435 (1970).
8. Wang, F. E. and Sutula, R. A., "On the Effects of Thermal Expansion in Metal Matrix Composites," J. Appl. Phys. 49, 944 (1978).
9. Hale, D. K., "The Physical Properties of Composite Materials," J. Mat. Sci. 11, 105-2142 (1976).
10. Schapery, R. A., "Thermal Expansion Coefficients of Composite Materials Based on Energy Principles," J. Comp. Mat. 2, 380 (1978).
11. Hill, R., "Theory of Mechanical Properties of Fiber-Strengthened Materials," J. Mech. Phys. Solids 12, 199 (1964); also, 13, 189-98 (1965).
12. Levin, V. M., "Thermal Expansion Coefficients of Heterogeneous Materials," Mekhanika Tverdogo Tela 2, 88-94 (1967).
13. Rosen, B. W. and Hashin, Z., "Effective Thermal Expansion Coefficients and Specific Heats of Composite Materials," Int. J. Engrg. Sci. 8, 157-173 (1970).

14. Hashin, Z., "Analysis of Fiber Composites with Anisotropic Constituents," J. Appl. Mech. 46, 543-549 (1979).
15. Halpin, J. C., "Stiffness and Expansion Estimates for Oriented Short Fiber Composites," J. Comp. Mat. 3, 732-734 (1969).
16. Wolff, E. G. and Eselun, S. A., "Thermal Expansion of a Boron-Aluminum Tube," J. Comp. Mat. 11, 30-32 (1977).
17. Dean, G. D., and Turner, P., "The Elastic Properties of Carbon Fibers and Their Composites," Composites, 174-180 (July 1973).
18. Whitney, J. M., "Elastic Moduli of Unidirectional Composites with Anisotropic Filaments," J. Comp. Mat. 1 188-193 (1967).
19. Kriz, R. D., and Stinchcomb, W. W., "Elastic Moduli of Transversely Isotropic Graphite Fibers and Their Composites," Exptl. Mech. 19, 41-49 (1979).
20. Neubert, H., TRW Space Systems, Redondo Beach, Calif., private communication.
21. Cooper, G. A. and Silwood, J. M., "Multiple Fracture in a Steel Reinforced Epoxy Resin Composite," J. Mat. Sci. 7, 325-333 (1972).
22. Garrett, R. W. and Bailey, J. E., "Multiple Transverse Fracture in 90° Cross Ply Laminates of a Glass Fiber Reinforced Polyester," J. Mat. Sci. 12, 157-168 (1977).
23. Eselun, S. A., Neubert, H. D., and Wolff, E. G., "Microcracking Effects on Dimensional Stability," SAMPE Symp. Proc. 24, 1299-1309 (1979).
24. Wolff, E. G., "Measurement Techniques for Low Expansion Materials," 9th National SAMPE Technical Conference, Atlanta, Georgia, 4-6 October 1977; in Conference Series 9, 57-72 (1977).
25. Wolff, E. G., and Eselun, S. A., "Double Michelson Interferometer for Contactless Thermal Expansion Measurements," SPIE Proc. 192 204-208 (1979).
26. Hawkins, G. F., The Aerospace Corp., El Segundo, Calif., private communication.
27. Kural, M. H. and Ellison, A. M., "Induced Errors during Thermal Expansion Testing of Graphite Fiber Reinforced Metal Matrix Composites," SAMPE Journal 16 (5), 20-26 (1980).

28. Sarka, B., Starke, E. A. and Pickens, J. O., "Effects of Processing on Monotonic and Cyclic Properties of Aluminum Alloy 6061 Reinforced with Sub-Micron Silicon Carbide Whiskers/Particles," February 1980, Program of 107th Annual Meeting AIME, Las Vegas, Nev., p. 189.
29. Skibo, M. D. and Hoover, W. R., "Stiffness and Strength of SiC-Al Composites," *ibid.*, p. 189.

LABORATORY OPERATIONS

The Laboratory Operations of The Aerospace Corporation is conducting experimental and theoretical investigations necessary for the evaluation and application of scientific advances to new military concepts and systems. Versatility and flexibility have been developed to a high degree by the laboratory personnel in dealing with the many problems encountered in the nation's rapidly developing space and missile systems. Expertise in the latest scientific developments is vital to the accomplishment of tasks related to these problems. The laboratories that contribute to this research are:

Aerophysics Laboratory: Launch and reentry aerodynamics, heat transfer, reentry physics, chemical kinetics, structural mechanics, flight dynamics, atmospheric pollution, and high-power gas lasers.

Chemistry and Physics Laboratory: Atmospheric reactions and atmospheric optics, chemical reactions in polluted atmospheres, chemical reactions of excited species in rocket plumes, chemical thermodynamics, plasma and laser-induced reactions, laser chemistry, propulsion chemistry, space vacuum and radiation effects on materials, lubrication and surface phenomena, photo-sensitive materials and sensors, high precision laser ranging, and the application of physics and chemistry to problems of law enforcement and biomedicine.

Electronics Research Laboratory: Electromagnetic theory, devices, and propagation phenomena, including plasma electromagnetics; quantum electronics, lasers, and electro-optics; communication sciences, applied electronics, semiconducting, superconducting, and crystal device physics, optical and acoustical imaging; atmospheric pollution; millimeter wave and far-infrared technology.

Materials Sciences Laboratory: Development of new materials; metal matrix composites and new forms of carbon; test and evaluation of graphite and ceramics in reentry; spacecraft materials and electronic components in nuclear weapons environment; application of fracture mechanics to stress corrosion and fatigue-induced fractures in structural metals.

Space Sciences Laboratory: Atmospheric and ionospheric physics, radiation from the atmosphere, density and composition of the atmosphere, aurorae and airglow; magnetospheric physics, cosmic rays, generation and propagation of plasma waves in the magnetosphere; solar physics, studies of solar magnetic fields; space astronomy, x-ray astronomy; the effects of nuclear explosions, magnetic storms, and solar activity on the earth's atmosphere, ionosphere, and magnetosphere; the effects of optical, electromagnetic, and particulate radiations in space on space systems.

THE AEROSPACE CORPORATION
El Segundo, California

0-8
DTIC